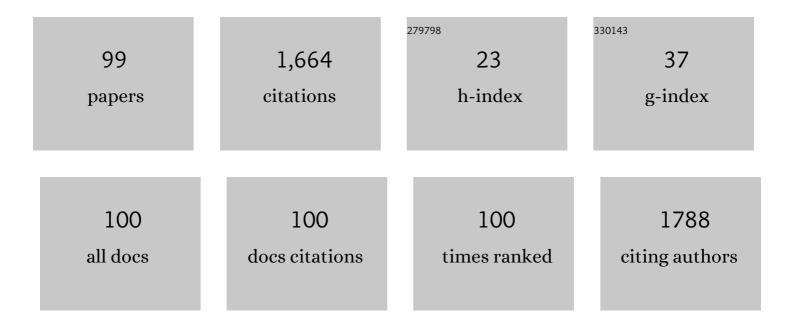
List of Publications by Year in descending order

Source: https://exaly.com/author-pdf/862395/publications.pdf Version: 2024-02-01



ROCEP 17EMD

#	Article	IF	CITATIONS
1	Non-interferometric photoacoustic remote sensing microscopy. Light: Science and Applications, 2017, 6, e16278-e16278.	16.6	150
2	Quantitative photoacoustic tomography with multiple optical sources. Applied Optics, 2010, 49, 3566.	2.1	97
3	Porphyrin Nanodroplets: Subâ€micrometer Ultrasound and Photoacoustic Contrast Imaging Agents. Small, 2016, 12, 371-380.	10.0	82
4	Top-orthogonal-to-bottom-electrode (TOBE) CMUT arrays for 3-D ultrasound imaging. IEEE Transactions on Ultrasonics, Ferroelectrics, and Frequency Control, 2014, 61, 266-276.	3.0	68
5	In-Vivo functional optical-resolution photoacoustic microscopy with stimulated Raman scattering fiber-laser source. Biomedical Optics Express, 2014, 5, 539.	2.9	67
6	Multi-wavelength photoacoustic imaging of inducible tyrosinase reporter gene expression in xenograft tumors. Scientific Reports, 2014, 4, 5329.	3.3	62
7	Deep non-contact photoacoustic initial pressure imaging. Optica, 2018, 5, 814.	9.3	54
8	Enhanced Detection of Cancer Biomarkers in Blood-Borne Extracellular Vesicles Using Nanodroplets and Focused Ultrasound. Cancer Research, 2017, 77, 3-13.	0.9	51
9	Glancing angle deposited nanostructured film Fabry-Perot etalons for optical detection of ultrasound. Optics Express, 2013, 21, 6391.	3.4	49
10	Detection of circulating tumor cells using targeted surface-enhanced Raman scattering nanoparticles and magnetic enrichment. Journal of Biomedical Optics, 2014, 19, 056014.	2.6	47
11	Top orthogonal to bottom electrode (TOBE) 2-D CMUT arrays for 3-D photoacoustic imaging. IEEE Transactions on Ultrasonics, Ferroelectrics, and Frequency Control, 2014, 61, 1393-1395.	3.0	40
12	Blood oxygen flux estimation with a combined photoacoustic and high-frequency ultrasound microscopy system: a phantom study. Journal of Biomedical Optics, 2012, 17, 036012.	2.6	37
13	Transparent capacitive micromachined ultrasonic transducer (CMUT) arrays for real-time photoacoustic applications. Optics Express, 2020, 28, 13750.	3.4	35
14	Ultraviolet photoacoustic remote sensing microscopy. Optics Letters, 2019, 44, 3586.	3.3	34
15	Double-SOI Wafer-Bonded CMUTs With Improved Electrical Safety and Minimal Roughness of Dielectric and Electrode Surfaces. Journal of Microelectromechanical Systems, 2012, 21, 668-680.	2.5	33
16	Multifrequency Interlaced CMUTs for Photoacoustic Imaging. IEEE Transactions on Ultrasonics, Ferroelectrics, and Frequency Control, 2017, 64, 391-401.	3.0	33
17	Transparent capacitive micromachined ultrasonic transducers (CMUTs) for photoacoustic applications. Optics Express, 2019, 27, 13204.	3.4	33
18	Reflective objective-based ultraviolet photoacoustic remote sensing virtual histopathology. Optics Letters, 2020, 45, 535.	3.3	33

#	Article	IF	CITATIONS
19	Engineering Dark Chromoprotein Reporters for Photoacoustic Microscopy and FRET Imaging. Scientific Reports, 2016, 6, 22129.	3.3	30
20	Temporal evolution of low-coherence reflectrometry signals in photoacoustic remote sensing microscopy. Applied Optics, 2017, 56, 5172.	2.1	28
21	Fabrication of Linear Array and Top-Orthogonal-to-Bottom Electrode CMUT Arrays With a Sacrificial Release Process. IEEE Transactions on Ultrasonics, Ferroelectrics, and Frequency Control, 2017, 64, 93-107.	3.0	27
22	Detecting rare cancer cells. Nature Nanotechnology, 2009, 4, 798-799.	31.5	25
23	Photoacoustic imaging of lymphatic pumping. Journal of Biomedical Optics, 2017, 22, 1.	2.6	23
24	In vivo photoacoustic difference-spectra imaging of bacteria using photoswitchable chromoproteins. Journal of Biomedical Optics, 2018, 23, 1.	2.6	23
25	Spectral analysis of the heart sounds in children with and without pulmonary artery hypertension. International Journal of Cardiology, 2014, 173, 92-99.	1.7	21
26	Self and Mutual Radiation Impedances for Modeling of Multi-Frequency CMUT Arrays. IEEE Transactions on Ultrasonics, Ferroelectrics, and Frequency Control, 2016, 63, 1441-1454.	3.0	19
27	Flexible transparent CMUT arrays for photoacoustic tomography. Optics Express, 2022, 30, 15877.	3.4	19
28	Multi-frequency CMUT arrays for imaging-therapy applications. , 2013, , .		18
29	Scattering cross-sectional modulation in photoacoustic remote sensing microscopy. Optics Letters, 2018, 43, 146.	3.3	18
30	Label-free lipid contrast imaging using non-contact near-infrared photoacoustic remote sensing microscopy. Optics Letters, 2020, 45, 4559.	3.3	18
31	Real-time functional photoacoustic remote sensing microscopy. Optics Letters, 2019, 44, 3466.	3.3	18
32	3D photoacoustic imaging using Hadamard-bias encoding with a crossed electrode relaxor array. Optics Letters, 2018, 43, 3425.	3.3	17
33	RNA Biomarker Release with Ultrasound and Phase-Change Nanodroplets. Ultrasound in Medicine and Biology, 2014, 40, 1847-1856.	1.5	16
34	Acoustic diagnosis of pulmonary hypertension: automated speech- recognition-inspired classification algorithm outperforms physicians. Scientific Reports, 2016, 6, 33182.	3.3	16
35	Transparent capacitive micromachined ultrasound transducer linear arrays for combined realtime optical and ultrasonic imaging. Optics Letters, 2021, 46, 1542.	3.3	16
36	Monitoring photodynamic therapy with photoacoustic microscopy. Journal of Biomedical Optics, 2015, 20, 106012.	2.6	15

#	Article	IF	CITATIONS
37	A Nonlinear Lumped Equivalent Circuit Model for a Single Uncollapsed Square CMUT Cell. IEEE Transactions on Ultrasonics, Ferroelectrics, and Frequency Control, 2019, 66, 1340-1351.	3.0	15
38	Multimodal imaging with spectral-domain optical coherence tomography and photoacoustic remote sensing microscopy. Optics Letters, 2020, 45, 4859.	3.3	15
39	S-sequence encoded synthetic aperture B-scan ultrasound imaging. , 2013, , .		14
40	Validating tyrosinase homologue <i>melA</i> as a photoacoustic reporter gene for imaging <i>Escherichia coli</i> . Journal of Biomedical Optics, 2015, 20, 106008.	2.6	13
41	Coherence-gated photoacoustic remote sensing microscopy. Optics Express, 2018, 26, 23689.	3.4	13
42	Dual-Frequency CMUT Arrays for Multiband Ultrasound Imaging Applications. IEEE Transactions on Ultrasonics, Ferroelectrics, and Frequency Control, 2021, 68, 2532-2542.	3.0	13
43	Virtual hematoxylin and eosin histopathology using simultaneous photoacoustic remote sensing and scattering microscopy. Optics Express, 2021, 29, 13864.	3.4	13
44	Simultaneous Azimuth and Fresnel Elevation Compounding: A Fast 3-D Imaging Technique for Crossed-Electrode Arrays. IEEE Transactions on Ultrasonics, Ferroelectrics, and Frequency Control, 2018, 65, 1657-1668.	3.0	12
45	In vivo combined virtual histology and vascular imaging with dual-wavelength photoacoustic remote sensing microscopy. OSA Continuum, 2020, 3, 2680.	1.8	12
46	Fast Orthogonal Row–Column Electronic Scanning Experiments and Comparisons. IEEE Transactions on Ultrasonics, Ferroelectrics, and Frequency Control, 2019, 66, 1093-1101.	3.0	11
47	Phase-function corrected diffusion model for diffuse reflectance of a pencil beam obliquely incident on a semi-infinite turbid medium. Journal of Biomedical Optics, 2013, 18, 067005.	2.6	10
48	S-sequence spatially-encoded synthetic aperture ultrasound imaging [Correspondence]. IEEE Transactions on Ultrasonics, Ferroelectrics, and Frequency Control, 2014, 61, 886-890.	3.0	10
49	CMUTs with improved electrical safety & minimal dielectric surface charging. , 2010, , .		9
50	Virtual histopathology with ultraviolet scattering and photoacoustic remote sensing microscopy. Optics Letters, 2021, 46, 5153-5156.	3.3	9
51	Detection of Heart Sounds in Children with and without Pulmonary Arterial Hypertension―Daubechies Wavelets Approach. PLoS ONE, 2015, 10, e0143146.	2.5	8
52	Mutual radiation impedance for modeling of multi-frequency CMUT arrays. , 2015, , .		8
53	Multimodality Raman and photoacoustic imaging of surface-enhanced-Raman-scattering-targeted tumor cells. Journal of Biomedical Optics, 2016, 21, 020503.	2.6	8
54	Synthetic aperture 3D ultrasound imaging schemes with S-sequence bias-encoded top-orthogonal-to-bottom-electrode 2D CMUT arrays. , 2013, , .		7

#	Article	IF	CITATIONS
55	Comparing Efficiency of micro-RNA and mRNA Biomarker Liberation with Microbubble-Enhanced Ultrasound Exposure. Ultrasound in Medicine and Biology, 2014, 40, 2207-2216.	1.5	7
56	F-mode ultraviolet photoacoustic remote sensing for label-free virtual H&E histopathology using a single excitation wavelength. Optics Letters, 2021, 46, 3500.	3.3	7
57	Modelling of large-scale multi-frequency CMUT arrays with circular membranes. , 2016, , .		6
58	Multimodal 3D photoacoustic remote sensing and confocal fluorescence microscopy imaging. Journal of Biomedical Optics, 2021, 26, .	2.6	6
59	Bias-sensitive transparent single-element ultrasound transducers using hot-pressed PMN-PT. OSA Continuum, 2021, 4, 2606.	1.8	6
60	Outperforming piezoelectric ultrasonics with high-reliability single-membrane CMUT array elements. Microsystems and Nanoengineering, 2022, 8, .	7.0	6
61	Reflection-mode multiple-illumination photoacoustic sensing to estimate optical properties. Photoacoustics, 2014, 2, 33-38.	7.8	5
62	Photoacoustic imaging of angiogenesis in a subcutaneous islet transplant site in a murine model. Journal of Biomedical Optics, 2016, 21, 066003.	2.6	5
63	Hadamard Aperiodic Interval Codes for Parallel-Transmission 2D and 3D Synthetic Aperture Ultrasound Imaging. Applied Sciences (Switzerland), 2022, 12, 4917.	2.5	5
64	Tissue perfusion rate estimation with compression-based photoacoustic-ultrasound imaging. Journal of Biomedical Optics, 2018, 23, 1.	2.6	4
65	Estimation of cerebral metabolic rate of oxygen consumption using combined multiwavelength photoacoustic microscopy and Doppler microultrasound. Journal of Biomedical Optics, 2018, 23, 1.	2.6	4
66	Fiber-based photoacoustic remote sensing microscopy and spectral-domain optical coherence tomography with a dual-function 1050-nm interrogation source. Journal of Biomedical Optics, 2021, 26, .	2.6	3
67	Toward wide-field high-speed photoacoustic remote sensing microscopy. , 2018, , .		3
68	Bias-sensitive crossed-electrode relaxor 2D arrays for 3D photoacoustic imaging. , 2018, , .		3
69	Enrichment and ratiometric detection of circulating tumor cells using PSMA- and folate receptor-targeted magnetic and surface-enhanced Raman scattering nanoparticles. Biomedical Optics Express, 2020, 11, 6211.	2.9	3
70	Fast hybrid optomechanical scanning photoacoustic remote sensing microscopy for virtual histology. Biomedical Optics Express, 2022, 13, 39.	2.9	3
71	S-sequence bias-encoded photoacoustic imaging with top Orthogonal to Bottom Electrode (TOBE) CMUT arrays. , 2013, , .		2
72	Non-invasive spinal vibration testing using ultrafast ultrasound imaging: A new way to measure spine function. Scientific Reports, 2018, 8, 9611.	3.3	2

#	Article	IF	CITATIONS
73	Towards microvascular pressure estimation using ultrasound and photoacoustic imaging. Photoacoustics, 2019, 14, 99-104.	7.8	2
74	A new photoacoustic method for measuring optical transport Green's functions in turbid media. , 2008, , .		1
75	Empirical model for dielectric charging in double-SOI-wafer-bonded CMUTs: Theory and experiment. , 2011, , .		1
76	Realtime flash-difference ultrasound imaging of phase-change perfluorocarbon nanodroplet activation. , 2012, , .		1
77	Electrical impedace matching of CMUT cells. , 2015, , .		1
78	A New 3D Imaging Technique Integrating Ultrafast Compounding, Hadamard Encoding, and Reconfigurable Fresnel Lensing, demonstrated on a 128-Element, Crossed Electrode Endoscope. , 2019, ,		1
79	Photoacoustic remote sensing 3D H&E histology with fluorescence validation. , 2021, , .		1
80	High sensitivity transparent capacitive micromachined ultrasound transducer linear arrays for optical, photoacoustic and ultrasound imaging. , 2021, , .		1
81	Single laser-shot super-resolution photoacoustic tomography with fast sparsity-based reconstruction. Photoacoustics, 2021, 22, 100258.	7.8	1
82	Investigation of photoacoustic signal strength as a function of scan-speed and laser-repetition-rate. , 2013, , .		0
83	Practical S-Sequence aperture coding schemes for volumetric imaging with Top Orthogonal to Bottom Electrode (TOBE) arrays. , 2015, , .		0
84	Nonlinear lumped modelling of large-scale CMUT TOBE architectures. , 2015, , .		0
85	S-sequence enhanced synthetic aperture ultrasound scattering tomography. , 2016, , .		Ο
86	Optimization strategies and neighbor pair complementary codes for massively parallel focal zone ultrafast ultrasound. , 2017, , .		0
87	Optimization strategies and neighbour-pair complementary codes for massively parallel focal-zone ultrafast ultrasound. , 2017, , .		0
88	A nonlinear large signal equivalent circuit model for a square CMUT cell. , 2017, , .		0
89	A nonlinear large signal equivalent circuit model for a square CMUT cell. , 2017, , .		Ο
90	Multi-frequency CMUT imaging arrays for multi-scale imaging and imaging-therapy applications. , 2017, ,		0

#	Article	IF	CITATIONS
91	Notice of Removal: Perfusion-rate estimation using compression-based photoacoustic-ultrasound imaging. , 2017, , .		Ο
92	Fabrication and performance of a 128-element crossed-electrode relaxor array, for a novel 3D imaging approach. , 2017, , .		0
93	Fabrication and performance of a 128-element crossed-electrode relaxor array, for a novel 3D imaging approach. , 2017, , .		Ο
94	A 30 MHz, 3D Imaging, Forward Looking Miniature Endoscope Based on a 128-Element Relaxor Array. , 2018, , .		0
95	Depth-resolved hematoxylin and eosin virtual histopathology with photoacoustic remote sensing and scattering microscopy. , 2021, , .		Ο
96	Fast analysis of resected breast tissue margins using ultraviolet photoacoustic remote sensing microscopy. , 2021, , .		0
97	Virtual histological assessment of human breast tumor specimens using spectral-domain optical coherence tomography augmented with ultraviolet photoacoustic remote sensing microscopy. , 2021, , .		Ο
98	Multi-layer label-free H&E-like histology using ultraviolet scattering-augmented photoacoustic remote sensing microscopy. , 2022, , .		0
99	Deep learning-enabled realistic virtual histology with ultraviolet scattering and photoacoustic remote sensing microscopy. , 2022, , .		Ο